

Effect of CO₂ exposure on the chemical stability and mechanical properties of BaZrO₃-ceramics

Rokas Sažinas, Carlos Bernuy-López, Mari-Ann Einarsrud and Tor Grande¹

¹Department of Materials Science and Engineering, Norwegian University of Science and Technology, NO-7491, Trondheim, Norway

Abstract

The reactivity of BaZrO₃ with CO₂ has been addressed as one of the major challenges with BaZrO₃-based electrolytes in proton ceramic fuel cells. Here, we present a study of the effect of CO₂ exposure of BaZrO₃-materials at elevated temperatures. Dense BaZr_{1-x}Y_xO_{3-δ} (x = 0, 0.05, 0.1, 0.2) and BaCe_{0.2}Zr_{0.7}Y_{0.1}O_{2.95} ceramics were prepared by conventional sintering of powder prepared by spray pyrolysis. The Vickers indentation method was used to determine the hardness and estimate the fracture toughness of pristine materials as well as the corresponding materials exposed to CO₂. Formation of BaCO₃ on the surface of exposed ceramics was confirmed by X-ray diffraction and electron microscopy. The reaction resulted in formation of Ba-deficient perovskite at the exposed surface. The reaction with CO₂ was most pronounced at 650 °C compared to the other temperatures applied in the study. The reactivity was also shown to depend on the Y-content and the grain size and was most pronounced for BaZr_{0.9}Y_{0.1}O_{3-δ}. The reaction with CO₂ was observed to have a profound effect on the fracture toughness of the ceramics, demonstrating a depression of the mechanical stability of the materials. The results are discussed with respect to the chemical and mechanical stability of BaZrO₃ materials, with particular emphasis on the composition and grain size.

Keywords: BaZrO₃, CO₂-reactivity, mechanical properties, stability

¹ Corresponding author: grande@ntnu.no

Introduction

Solid oxide fuel cells (SOFC) have during the last decades gained considerable attention in relation to power generation or combined heat and power devices due to their high-energy conversion efficiency.¹⁻⁴ Recent advances of SOFCs have resulted in reduced operation temperatures, which has enabled the use of metallic interconnects and improved the stability as well as the durability.^{3, 4} Protonic ceramic fuel cells (PCFC) based on proton conducting electrolytes with superior ionic conductivity, may lead to even lower operating temperatures and improved performance since in this configuration the exhaust water is produced at the air electrode and thereby not diluting the fuel at the fuel electrode side.⁴ SOFCs can also be operated as electrolyzers by reversing the voltage, and the prospects of electrolyzers based on SOFC technology has become an important research field.⁵⁻⁷

The most promising proton conducting electrolytes are $\text{BaCe}_{1-x}\text{Y}_x\text{O}_{3-x/2}$ (BCY)^{4, 8-11} and $\text{BaZr}_{1-x}\text{Y}_x\text{O}_{3-x/2}$ (BZY),¹²⁻¹⁶ which exhibit high proton conductivity at intermediate temperatures (~ 500 °C)¹⁷. Despite the encouraging proton conductivity of these materials, there are several issues addressed related to their chemical stability, mechanical properties and difficulties in sintering of BZY.^{15, 17} BCY has a low chemical stability due to the reactivity with CO_2 ¹⁸ resulting in formation of barium carbonate,¹⁹⁻²⁵ while BZY is proposed to exhibit sufficient chemical stability in CO_2 -containing atmosphere.^{12, 24-29} The reactivity with CO_2 will result in degradation, which precludes applications in electrochemical devices such as fuel cells based on hydrocarbon fuels. The stability of $\text{Ba}(\text{Zr,Ce})_{1-x}\text{Y}_x\text{O}_{3-x/2}$ in CO_2 atmosphere is increasing with increasing Zr content according to thermodynamic data,^{25, 27} and can be rationalized by the higher acidity of ZrO_2 relative to CeO_2 .^{13, 21, 22, 27} Finally, although decomposition of BaZrO_3 is expected below ~ 530 °C in pure CO_2 (1 atm),²² BaZrO_3 has been reported to be stable below this temperature due to slow kinetics of the reaction with CO_2 .

Here we report on the effect of CO_2 exposure on the chemical stability and mechanical performance of $\text{BaZr}_{1-x}\text{Y}_x\text{O}_{3-x/2}$ ($x = 0, 0.05, 0.1, \text{ and } 0.2$) and $\text{BaCe}_{0.2}\text{Zr}_{0.7}\text{Y}_{0.1}\text{O}_{2.95}$. Modifications in the microstructure and formation of carbonates at the surface of the ceramics were investigated by electron microscopy and X-ray diffraction. Vickers indentation was for the first time applied to investigate the degradation of the mechanical performance due to reaction with CO_2 . Degradation associated with BaCO_3 formation was demonstrated, and the consequences for the mechanical stability of BaZrO_3 -based electrolytes are discussed.

Experimental

Sample preparation and exposure to CO₂

Fine ceramic powders with composition BaZr_{1-x}Y_xO_{3-x/2} (x = 0, 0.05, 0.1, and 0.2), denoted as BZ, BZY5, BZY10, and BZY20 respectively and BaCe_{0.2}Zr_{0.7}Y_{0.1}O_{2.95} (BCZY27) were prepared by aqueous nitrate solution spray pyrolysis (CerPoTech AS, Trondheim, Norway). The as-pyrolyzed powders were calcined at 950 °C for 12 h in air and ball milled with yttria stabilized zirconia (YSZ) balls in isopropanol for 72 h, dried at 200 °C for 24 h in ambient air, ground and sieved (150 μm). Green cylindrical pellets with 10 mm diameter and ~3 mm thickness were made by uniaxial pressing at 100 MPa with subsequent cold isostatic pressing (CIP) at 200 MPa giving final green densities of 55–56 % of theoretical. Sintering of the pellets was performed in a muffle furnace at 1600 °C for 10 h in ambient air with a heating rate of 600 °C/h. The samples denoted BZY10_1700 and BCZY27_1700 were in addition thermally annealed at 1700 °C for 10 h after sintering at 1600 °C. Samples denoted BZY10_1600* and BCZY27_1600* were sintered using sacrificial powder at 1600 °C for 10 h in air. The sacrificial powder consisted of BZY20, prepared from stoichiometric amounts of oxides via solid state reaction at 1400 °C for 10 h, and ~10 wt% of BaCO₃ (ACS Reagent, ≥99 %, Sigma-Aldrich). The surface of the sintered specimens was polished with SiC papers and diamond suspensions down to 1 μm to obtain smooth surfaces for Vickers indentation. The sintering conditions for the different samples are summarized in Table 1. The polished samples were exposed to CO₂ (< 50 ppm H₂O) at constant flow (~1 atm) for 10 or 20 h in an alumina tube furnace (Entech ETF 50/17-S) at temperatures from 500 to 750 °C. The heating and cooling rates were 300 °C/h. Corresponding heat treatment of all the materials was also performed at 650 °C for 10 h in dry synthetic air.

Materials characterization

X-ray powder diffraction (XRD) of calcined powders and sintered materials was performed on a D8 Advance DaVinci diffractometer using CuK_{α1}. The diffraction patterns were recorded in the range 20° ≤ 2θ ≤ 60° with a scanning rate 0.7° min⁻¹. Rietveld refinement of the XRD patterns for powders was carried out using the TOPAS V4.1 using a cubic structure model (*Pm* $\bar{3}$ *m*) for all the materials. Grazing incident XRD (GIXD) was performed using D8 Advance DaVinci diffractometer using CuK_{α1} and parallel beam optics.

The density of the materials was measured by the Archimedes method using isopropanol. The microstructure before and after Vickers indentation were investigated with Hitachi S3400N and Hitachi FEG Zeiss Ultra JEOL840 scanning electron microscopes (SEM) on gold coated samples. The average grain size of the ceramics was estimated by the linear intercept method of 50-60 grains from SEM images of polished and thermally etched (0.25 h, 1400 °C) surfaces. BZY5 and BZY10 samples were etched at 1450 °C for 15 min. The chemical composition of phases was investigated by Energy dispersive spectroscopy (EDS) with Oxford Instruments AZtec Energy analysis software.

Mechanical properties of dense and polished ceramics were investigated by the Vickers micro-indentation technique (Leica VMHT MOT) using loads of 0.1, 0.15, 0.25, 0.5, 1, 2 and 5 N. Distance between each indentation was kept more than 5 times the diagonal of the indent and load holding time was set to 10 s. The Vickers hardness was calculated applying geometrical measurements of indent size from SEM images at each load using equation (1),³⁰

$$H_v = 1.8544 \frac{P}{d^2} \quad (1)$$

where P is the applied load (kg) and d is the mean length of diagonals (mm). The fracture toughness of the materials was estimated using normalized Niihara's equation (2),³¹

$$K_{IC} = 9.518 \left(\frac{c}{a} \right)^{-1.5} (H_v^{0.6})(a^{0.5}) \quad (2)$$

where K_{IC} , is the fracture toughness (MPa·m^{1/2}); a is 1/2 of indentation diagonal length (m); c is 1/2 of radial crack length (m) and H_v is the measured Vickers hardness (MPa). The choice of using Niihara's equation (eq. 2) was based on the criteria $c/a > 2.5$ where c is the radial surface crack radius and a is the half diagonal of the Vickers indent. It is important to note that the Vickers indentation test does not provide fracture toughness data sufficient for a reliable test,³² but gives a good estimate of relative changes in the fracture toughness.

Results

Pristine materials

The powders calcined at 950 °C for 12 h in air were all phase pure according to XRD, revealing that this temperature was sufficient to remove traces of BaCO₃ in the as-prepared powders. This calcination temperature is lower than applied in a previous study using similar powders prepared by spray pyrolysis³³. In the previous study the particle size was ~100 nm after calcination at 1000 °C, inferring that the present particle size in this study was lower than 100 nm due to the lower calcination temperature. The sintering temperature and time were varied in order to obtain high density of the ceramics, and the optimized sintering conditions are given in Table 1. All the materials achieved densities higher than 94 % relative to the theoretical density calculated from the unit cell parameters found by Rietveld refinements (Table 1). Increasing the heating rate from 200 to 600 °C/h had a profound effect on the final density, while no significant improvement in the relative density could be obtained by increasing the sintering time from 10 h to 16 h or using sacrificial powder. The final relative density and grain size of the materials using 600 °C/h heating rate are included in Table 1.

SEM images of the polished and thermally etched surface of BaZrO₃, BaZr_{1-x}Y_xO_{3-x/2} and BCZY27 pellets sintered at 1600 °C for 10 h in air are shown in Fig. 1. The Y-doped barium zirconates have smaller grains than pure BaZrO₃, while the grain size is increasing with Y-content in BZY. BZY5 had the smallest grain size of 0.18 μm. The grain size of BZY10_1600 and BCZY27_1600 was around 0.25 μm, while grain growth to 0.6 μm was induced after thermal annealing at 1700 °C (Table 1). The average grain size increased on sintering using sacrificial powder (Table 1).

The BZY10 and BZY20 ceramics conventionally sintered at 1600 °C for 10 h in air contained a minor amount of cubic Y₂O₃ phase detected by XRD due to loss of BaO. The Y₂O₃ content in BZY10 and BZY20 was estimated to 1.0 and 2.0 wt%. Y₂O₃ was not present in these two materials sintered with sacrificial powder, but only BZY10* was investigated with respect to reaction with CO₂.

Vickers micro-indentation method

A SEM image of a typical indent in pristine BCZY27 is shown in Fig. 2, demonstrating clearly the cracks propagating from the four corners of the indent. In all the pristine materials the crack propagated by an intergranular mode both in the initial and final part of the crack.

The Vickers hardness of BZY10 as a function of the load is shown in Fig. 3. The hardness converged towards a constant value with increasing load in line with theory³⁴⁻³⁷. Loads higher than 5 N induced lateral cracks and could not give reasonable measurement of the Vickers hardness and cracks with well-defined lengths. A similar trend as shown in Fig. 3 was observed for all other compositions (not shown). Based on these observations a load of 2 N was used for all the following measurements on all the materials. Ideally, hardness should be measured using a load which would not give radial cracks, but this was only obtained for low loads (<0.25 N) resulting in strongly distorted indents. Vickers hardness for all the pristine materials measured using 2 N load is summarized in Table 1.

The effect of the indentation load on the estimated fracture toughness of pristine BZY10 using Eq. 2 is also shown in Fig. 3 (insert). The fracture toughness was not changing significantly with variation in the load above 1 N. The fracture toughness could not be calculated at 0.1 and 0.15 N loads because the crack lengths were too small. The same trends were observed for all materials. The fracture toughness for the pristine ceramics measured using 2 N load is summarized in Table 1.

The Vickers hardness and fracture toughness of the pristine BZY materials are decreasing with the Y-content accompanied with increasing lattice parameters and oxygen vacancy concentration (Table 1). Moreover, the grain size of the BZY materials was slightly increasing with increasing the Y-content. Vickers hardness was marginally improved for BZY10 by increasing the grain size (BZY10_1700), while the opposite effect was observed for BCZY27 (BCZY27_1700). On the other hand, fracture toughness of both compositions decreased after annealing at 1700 °C. There was an apparent reduction in Vickers hardness and fracture toughness of the samples sintered using sacrificial powder (BZY10_1600* and BCZY27_1600*). BaZrO₃ ceramics with the largest grains (~1 μm) possess moderate hardness and fracture toughness compared to the BZY materials.

Chemical and mechanical stability of $BaZr_{1-x}Y_xO_{3-x/2}$ and $BaCe_{0.2}Zr_{0.7}Y_{0.1}O_{2.95}$ in CO_2

SEM images of indents in pristine BZY10 and BZY10 exposed to CO_2 for 10 h at different temperatures are shown in Fig. 4. Relatively large crystals with average size $\sim 3 \mu m$ (see inset Fig. 4c) are evident on the surface of the exposed material. EDS confirmed that the crystals consisted of Ba, C and O, and XRD confirmed that the crystals were $BaCO_3$ (Fig. 5). No additional crystalline phase could be observed using grazing incidence XRD (Fig. 5). The formation $BaCO_3$ on the surface took place from 550 to 750 °C (Fig. 4), while the maximum amount of $BaCO_3$ was observed at 650 °C.

A polished cross section of BZY10 after exposure to CO_2 is shown in Fig. 6. EDS line scans of Zr, Ba and Y revealed a gradient in the element content towards the surface exposed to CO_2 . A clear decrease in the Ba-content is evident at the surface, while the Zr and Y-contents are increasing. The data point to changes in the Ba/Zr ratio in the perovskite towards the surface exposed to CO_2 .

SEM images of the surfaces of $BaZr_{1-x}Y_xO_{3-x/2}$ ($x = 0, 0.05, 0.1, 0.2$) and $BaCe_{0.2}Zr_{0.7}Y_{0.1}O_{3-\delta}$ after exposure to CO_2 at 650 °C for 10 h are shown in Figs. 4, 7 and 8. These images demonstrate that the size and number density of the $BaCO_3$ crystals on the material surfaces depended on both the microstructure and the composition of the ceramic. A larger amount of smaller $BaCO_3$ crystals were formed on BZY20 compared to BZY10. The reaction with CO_2 with BCZY27 resulted in a few relatively large $BaCO_3$ crystals, inferring that the rate of nucleation of $BaCO_3$ is low compared to the growth rate. The images of the surface of BZY10_1600* and BCZY27_1600* ceramics demonstrate that the use of sacrificial powder during sintering reduces the amount of $BaCO_3$ crystals formed in CO_2 at 650 °C (Fig. 8). Formation of $BaCO_3$ could not be observed by SEM in case of pure $BaZrO_3$ but was confirmed by grazing incident XRD (not shown), and the Vickers indent in the exposed materials was altered relative to indent in the pristine material (Fig. 7a). Finally, the cracks in samples exposed to CO_2 (Fig. 4, 7 and 8) propagated both along grain boundaries as well as throughout the grains (transgranular mode).

The Vickers hardness and the fracture toughness of BZY10 and BCZY27 with CO_2 exposure temperature are shown in Fig. 9. The Vickers hardness of BZY10 and BCZY27 did not change significantly due to exposure to CO_2 (Fig. 9a and 9c). On the other hand, fracture toughness of

the BZY10 is clearly decreasing with increasing exposure temperature (see Fig. 9b). The reduced toughness was most pronounced for BZY10_1700 with the largest grain size. The fracture toughness of BCZY27 clearly decreases with increasing exposure temperature in line with the corresponding data for BZY10 (Fig. 9d). The Vickers hardness and fracture toughness of BZY10_1600* and BCZY27_1600* sintered at 1600 °C with sacrificial powder and exposed to CO₂ at 650 °C (Fig. 9) are lower relative to the samples sintered without sacrificial powder. The reduction in the fracture toughness does not reflect the amount of BaCO₃ crystals formed at the surface (see Figs. 4, 7 and 8).

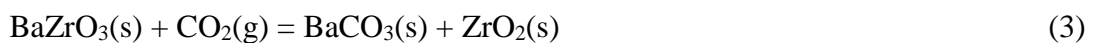
The dependence of the Vickers hardness and the fracture toughness of BaZr_{1-x}Y_xO_{3-x/2} and BaCe_{0.2}Zr_{0.7}Y_{0.1}O_{2.95} on the heating temperature in pure CO₂ are shown in Fig. 10. The hardness of the materials remains relatively constant and was not greatly affected by the formation of BaCO₃. The lengths of the lateral cracks were observed to increase with exposure temperature for all the compositions and consequently the fracture toughness of the materials decreased. Fig. 10 implies that BZY5 with the smallest grains show the most profound reduction in fracture toughness among the acceptor doped materials. The fracture toughness of BaZrO₃ was also shown to be strongly reduced by exposure to CO₂.

The Vickers hardness and fracture toughness of all materials exposed to synthetic air at 650 °C for 10 h are summarized in Table 1 and Fig. 10. The Vickers hardness and fracture toughness of these materials did not deviate from the properties of the pristine materials, which demonstrated that solely the thermal treatment does not influence the hardness and fracture toughness. We can therefore conclude that the observations reported for the materials exposed to CO₂ are truly an effect of the chemical reaction with CO₂.

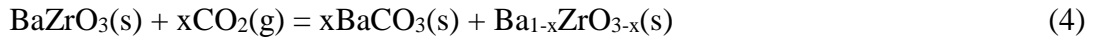
Discussion

Formation of BaCO₃ and chemical stability of BZY-materials

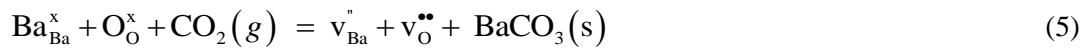
The reaction taking place at the surface, using pure BaZrO₃ as an example, has previously been proposed to be



Despite substantial efforts by diffraction and microscopy we could not detect any evidence for the formation of ZrO_2 . In contrast a concentration gradient towards the surface exposed to CO_2 could be observed by EDS (Fig. 6). An alternative reaction could therefore be established where the formation of Ba resulted in the formation of Ba-deficient $BaZrO_3$. The reaction taking place at the surface during CO_2 exposure, using pure $BaZrO_3$ as an example, is then proposed to



Alternatively, reaction (4) can be formulated using point defects as

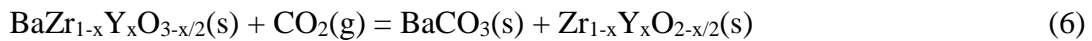


The energetics of vacancy formation $BaZrO_3$ has been studied first principle calculations, showing Ba-vacancies has the lowest formation energy relative to the other point defects supporting reaction (4).³⁸ An illustration of the reaction is shown in Fig. 11. $BaCO_3$ crystals grow on the surface due to mobility of Ba^{2+} , while Zr (Y) with inferred lower mobility, remains in the crystal structure forming $Ba_{1-x}ZrO_{3-x}$. Rietveld refinement of the conventional XRD patterns of the ceramics after exposure to CO_2 did not show any change in the lattice parameters of the BZY materials, Gracing incident XRD of $BaZrO_3$ and BZY10 after CO_2 exposure revealed however a minor shift the cell from 4.193 to 4.190 and 4.198 to 4.196, respectively (the uncertainty in the unit cell parameters obtain from GIXRD is larger than conventional XRD). The downshift in the unit cell parameter give supporting evidence for the formation of Ba-deficient BZY at the surface.³⁹ The Ba-deficiency induced by the reaction with CO_2 could in principle result in segregation of Y_2O_3 or Y incorporation into the Ba-site.³⁹ Formation of Y_2O_3 due to the reaction is not likely based on the EDS data on the surface (Fig. 6), while Y on Ba site cannot be proven nor disregarded based on the data provided in this study. Based on the estimated amount of $BaCO_3$ crystal on the surface on BZY10 the Ba-deficiency was estimated to be $Ba_{0.92}Zr_{0.9}Y_{0.1}O_{2.87}$ assuming that the reaction influenced only a $\sim 1 \mu m$ layer of the material ($x \sim 0.08$ for reaction (4)).

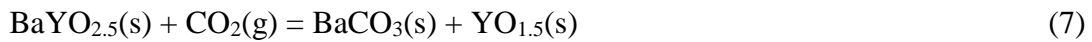
Formation of $BaCO_3$ on the surface of the BZY and BCZY27 ceramics (Fig. 4, 7 and 8) reduced clearly the fracture toughness (Figs. 9 and 10). Reaction (4) was most pronounced at $650 \text{ }^\circ C$

where the surface morphology was also most strongly modified by growth of large crystals of BaCO₃, which was most likely nucleated at the grain boundaries. The effect on the fracture toughness was even more pronounced above 650 °C (Fig. 10). The reaction with CO₂ is therefore also likely even at temperatures as high as 750 °C.

Assuming reaction (3) to be dominant the reaction between BaZr_{1-x}Y_xO_{3-x/2} and CO₂ can be expressed as



The Gibbs energy of reaction (6) can be estimated in terms of the Gibbs energy of reaction (3) and the following hypothetical reaction



where $\Delta G^\circ\{6\} = (1-x)\Delta G^\circ\{3\} + x\Delta G^\circ\{7\}$. $\Delta G^\circ\{3\}$ and $\Delta G^\circ\{7\}$ can be estimated from literature data.^{18, 19, 40, 41} The Gibbs energy can be expressed as a function of the partial pressure of CO₂ through the expressions

$$\Delta G^\circ\{6\} = \Delta H^\circ\{6\} - T\Delta S^\circ\{6\} = -RT\ln K_5 = -RT\ln(p\text{CO}_2)^{-1} \quad (8)$$

The relationship between $p\text{CO}_2$ and the temperature at equilibrium is then given by

$$\ln(p\text{CO}_2) = (\Delta H^\circ\{6\}/R)(1/T) - \Delta S^\circ\{6\}/R \quad (9)$$

The stable region for BZY materials can be calculated from equation (9). The result is shown in Fig.12a. The lines represent boundaries separating the stable and unstable regions with respect to reaction with CO₂. The thermodynamic stability of BZY decreases with increasing Y-content as particularly shown in Fig. 12b. Although reaction (3) does not represent the true reaction with CO₂, Fig. 12 illustrates how the relative stability of BaZrO₃ changes with respect to Y-doping. Moreover, it is known that the introduction of Ce⁴⁺ in BaZrO₃ attenuates the thermodynamic stability.^{22, 25} Corresponding thermodynamic data for other dopants than Y would be very interesting with respect to the thermodynamic stability of BaZrO₃ with respect to doping.

We infer that kinetics of the reaction with CO₂ also plays an important role. The effects which could influence on the heterogeneous phase equilibria are acceptor doping (vacancy concentration), cerium content as well as grain size of the ceramics. It is inferred from reaction (4) that the kinetics of the reaction is also related to the cation mobility in BaZrO₃-materials. The chemical reaction is most likely to occur at the grain boundaries because the cations are usually more mobile on the grain boundaries than in the bulk.⁴²

The reactivity of BZY-based materials with CO₂ reported in this study is novel with regards to previous attempts to study the reaction with CO₂.^{4, 12, 22, 27} The reaction proposed in this study is also new and does involve the formation of Ba-deficient perovskite. In these studies BZY-ceramics were concluded to be chemically stable in CO₂ atmosphere, in contradiction with the data provided in this study. It is noteworthy that the experiments were conducted in 1 atm CO₂ and should be considered as harsh. Lower partial pressures of CO₂ will increase the stability region of the BZY materials (see Fig. 12b).^{4, 22, 25, 27} This work is also the first study demonstrating the effect reaction with CO₂ on the mechanical performance.

Methodology (Vickers micro-indentation)

The mechanical performance of ceramics can be revealed by the Vickers micro-indentation method based on the size of indents and radial cracks.^{34, 35} A typical indent on a solid is illustrated in the inset in Fig. 2. Both the indentation fracture load and load holding time can be varied. A previous report on Vickers indentation in zirconia demonstrated that 10 s holding time was sufficient to obtain stable indent,³⁵ and this time was adopted in this study. The loads were varied in the range 0.25–5 N. Low loads (< 0.25 N) resulted in distorted indent shape and the loads < 1 N resulted in higher Vickers hardness values, whereas high loads (> 5 N) induced lateral cracks. Most of the data reported here was therefore measured using 2 N where the indent was both, symmetrical and with radial cracks propagating from all four corners. The fracture toughness calculated using eq. 2^{31, 32} does not provide the same accuracy as methods like SEVNB.³⁶ However, the method gives a good measure of the relative changes in the fracture toughness and provides insight in the change in the mechanical performance of the materials due to exposure to CO₂.

The presence of relatively large BaCO₃ crystals on the surface will affect the uncertainty in the measured hardness and apparent increase in hardness was estimated from the indents. The reason for this is that the surface morphology is modified from the initial smooth flat surface

due to the reaction with CO₂. During indentation these BaCO₃ crystals were crushed, reducing the indentation diagonal length resulting in an apparently increasing hardness. We have not made any attempts to correct for this systematic error in the hardness.

Hardness and fracture toughness of pristine BZY-based materials

Hardness of a material depends on the bonding strength, Young's modulus, grain size, porosity, surface roughness, and possibly also mechanically induced stress on the surface of the materials after polishing.³⁷ The hardness as a function of applied load has a softening effect at low loads, which is a well-known effect in ceramics.³⁷ According to our results, there is no systematic variation in the Vickers hardness with regards to the grain size and acceptor dopant concentration for the pristine materials. The Vickers hardness of the BZY10 and BCZY27 samples sintered with sacrificial powder is lower compared to the samples sintered by conventional sintering. This is most likely related to the presence of minor amount of Y₂O₃ in the conventionally sintered ceramics. Finally, the reported hardness of materials reported in this study is in good agreement with the hardness reported for similar materials.⁴³⁻⁵⁰

The fracture toughness of the conventionally sintered pristine materials does not have a systematic variation with regards to the grain size or the acceptor dopant level. It is noteworthy, that the fracture toughness decreased in the BZY10 and BCZY27 ceramics containing larger grains after sintering with sacrificial powder (Table 1). Possible explanations for these observations are the increased grain size and suppression of formation of Y₂O₃ secondary phase due to a lower BaO loss by using the sacrificial powder.

Mechanical stability of BaZr_{1-x}Y_xO_{3-x/2} and BaCe_{0.2}Zr_{0.7}Y_{0.1}O_{2.95} in CO₂

The cracks propagated by an intergranular mode in the pristine materials. However, when the samples were heat treated in pure CO₂, the cracks propagated along grain boundaries as well as throughout the grains (see Fig. 6). The reaction with CO₂ does therefore indeed change the mechanical properties of the materials.

In the following a qualitative discussion of the chemical and mechanical stability of the BZY-based materials is given. The significant change in phase composition due to the reaction with CO₂ may induce mechanical stress at the surface. A considerable strain induced stress during chemical expansion due to hydration/dehydration was recently addressed for BZY-materials.^{51,}

⁵² During operation of a fuel cell the level of the stress will additionally depend on the gradient

in the concentration of the water or protons as they diffuse from the surface to the interior of a material. The stress induced at the surface during reaction with CO₂ is reflected by the reduced fracture toughness reported here. Reduction in fracture toughness reveals reduction in fracture strength of the materials.⁵³ We therefore argue that chemical stability of proton conductors like BZY is most critical with respect to mechanical failure due to decomposition at elevated temperatures. The chemical reaction with CO₂ was significant in the temperature interval 550–750 °C. This will lead to microstructural changes at the interface between electrolyte and electrodes in fuel cells. The reduced fracture toughness is most likely related to the weakening of the grain boundaries due to the reaction with CO₂. In coarse-grained ceramics chemically induced stress induces micro-cracking, reduced mechanical strength, and possibly catastrophic failure. Some of the problems with low mechanical performance of proton-conducting oxides⁴ may therefore be related to micro-cracking induced by reaction with CO₂. Consequently, care must be taken if BZY-based materials will be applied in environments containing significant vapor pressures of CO₂.

Conclusions

Dense and phase pure Y³⁺- and Ce⁴⁺-doped barium zirconate ceramics, BaZr_{1-x}Y_xO_{3-δ} (x = 0, 0.05, 0.1, 0.2) and BaCe_{0.2}Zr_{0.7}Y_{0.1}O_{2.95}, were successfully prepared from powders prepared by spray pyrolysis. The stability of these ceramics was investigated by exposing the materials to pure CO₂ atmosphere. Clear evidence for the formation of BaCO₃ was provided by X-ray diffraction and microscopy for all materials. The reaction with CO₂ resulted in formation of Ba-deficient perovskite at the exposed surface. Significant reduction of the fracture toughness was observed for all the materials due to CO₂ exposure in the temperature range 550–750 °C. The reaction of BaZrO₃-based materials with CO₂ is discussed in relation to application of proton conducting materials based on BZY as electrolytes in intermediate temperature proton conducting fuel cells.

Acknowledgments

Financial support from The Research Council of Norway under the program NANO2021 to the project (Number 228355) "Functional oxides for clean energy technologies: fuel cells, gas separation membranes and electrolyzers" (FOXCET) conducted by SINTEF Materials and

Chemistry, University of Oslo and The Norwegian University of Science and Technology (NTNU) in Trondheim, is gratefully acknowledged.

References

- ¹S. M. Haile, "Fuel cell materials and components," *Acta Mater.*, **51**, 5981-6000 (2003).
- ²B. C. H. Steele, and A. Heinzl, "Materials for fuel-cell technologies," *Nature*, **414**, 345-52 (2001).
- ³M. Liu, M. E. Lynch, K. Blinn, F. M. Alamgir, and Y. Choi, "Rational SOFC material design: new advances and tools," *Materials Today*, **14**, 534-46 (2011).
- ⁴K. D. Kreuer, "Proton-conducting oxides," *Ann. Rev. Mater. Res.*, **33**, 333-59 (2003).
- ⁵M. A. Laguna-Bercero, "Recent advances in high temperature electrolysis using solid oxide fuel cells: A review," *J. Pow. Sour.*, **203**, 4-16 (2012).
- ⁶S. D. Ebbesen, S. H. Jensen, A. Hauch, and M. B. Mogensen, "High Temperature Electrolysis in Alkaline Cells, Solid Proton Conducting Cells, and Solid Oxide Cells," *Chem. Rev.*, **114**, 10697-734 (2014).
- ⁷C. Graves, S. D. Ebbesen, S. H. Jensen, S. B. Simonsen, and M. B. Mogensen, "Eliminating degradation in solid oxide electrochemical cells by reversible operation," *Nat. Mater.*, **14**, 239-44 (2015).
- ⁸H. Iwahara, H. Uchida, K. Ono, and K. Ogaki, "Proton Conduction in Sintered Oxides Based on BaCeO₃," *J. Electrochem. Soc.*, **135**, 529-33 (1988).
- ⁹T. Shimura, H. Tanaka, H. Matsumoto, and T. Yogo, "Influence of the transition-metal doping on conductivity of a BaCeO₃-based protonic conductor," *Solid State Ionics*, **176**, 2945-50 (2005).
- ¹⁰T. Schober, F. Krug, and W. Schilling, "Criteria for the application of high temperature proton conductors in SOFCs," *Solid State Ionics*, **97**, 369-73 (1997).
- ¹¹B. Zhu, X. Liu, and T. Schober, "Novel hybrid conductors based on doped ceria and BCY20 for ITSOFC applications," *Electrochem. Comm.*, **6**, 378-83 (2004).
- ¹²H. Iwahara, T. Yajima, T. Hibino, K. Ozaki, and H. Suzuki, "Protonic conduction in calcium, strontium and barium zirconates," *Solid State Ionics*, **61**, 65-9 (1993).
- ¹³K. D. Kreuer, "Aspects of the formation and mobility of protonic charge carriers and the stability of perovskite-type oxides," *Solid State Ionics*, **125**, 285-302 (1999).
- ¹⁴T. Schober, and H. G. Bohn, "Water vapor solubility and electrochemical characterization of the high temperature proton conductor BaZr_{0.9}Y_{0.1}O_{2.95}," *Solid State Ionics*, **127**, 351-60 (2000).
- ¹⁵P. Babilo, T. Uda, and S. M. Haile, "Processing of yttrium-doped barium zirconate for high proton conductivity," *Journal of Materials Research*, **22**, 1322-30 (2007).
- ¹⁶Y. Yamazaki, R. Hernandez-Sanchez, and S. M. Haile, "High Total Proton Conductivity in Large-Grained Yttrium-Doped Barium Zirconate," *Chem. Mater.*, **21**, 2755-62 (2009).
- ¹⁷W. G. Coors, "Protonic ceramic fuel cells for high-efficiency operation with methane," *J. Pow. Sour.*, **118**, 150-6 (2003).
- ¹⁸S. Gopalan, and A. V. Virkar, "Thermodynamic Stabilities of SrCeO₃ and BaCeO₃ Using a Molten-Salt Method and Galvanic Cells," *J. Electrochem. Soc.*, **140**, 1060-5 (1993).
- ¹⁹M. J. Scholten, J. Schoonman, J. C. van Miltenburg, and H. A. J. Oonk, "Synthesis of strontium and barium cerate and their reaction with carbon dioxide," *Solid State Ionics*, **61**, 83-91 (1993).
- ²⁰K. D. Kreuer, "On the development of proton conducting materials for technological applications," *Solid State Ionics*, **97**, 1-15 (1997).
- ²¹A. Demin, P. Tsiakaras, E. Gorbova, and S. Hramova, "A SOFC based on a co-ionic electrolyte," *J. Pow. Sour.*, **131**, 231-6 (2004).
- ²²D. Medvedev, J. Lyagaeva, S. Plaksin, A. Demin, and P. Tsiakaras, "Sulfur and carbon tolerance of BaCeO₃-BaZrO₃ proton-conducting materials," *J. Pow. Sour.*, **273**, 716-23 (2015).
- ²³E. H. P. Cordfunke, A. S. Booiij, and M. E. Huntelaar, "The thermochemical properties of BaCeO₃(s) and SrCeO₃(s) from T = (5 to 1500) K," *J. Chem. Thermodynamics*, **30**, 437-47 (1998).
- ²⁴I. Barin, *Thermochemical Data of Pure Substances*. (VCH, Weinheim, 1998), pp. 3rd edition.

- ²⁵D. Medvedev, A. Murashkina, E. Pikalova, A. Demin, A. Podias, and P. Tsiakaras, "BaCeO₃: Materials development, properties and application," *Prog. Mater. Sci.*, **60**, 72-129 (2014).
- ²⁶K. T. Jacob, and Y. Waseda, "Potentiometric determination of the gibbs energies of formation of SrZrO₃ and BaZrO₃," *MMTB*, **26**, 775-81 (1995).
- ²⁷K. H. Ryu, and S. M. Haile, "Chemical stability and proton conductivity of doped BaCeO₃-BaZrO₃ solid solutions," *Solid State Ionics*, **125**, 355-67 (1999).
- ²⁸J.-S. Park, J.-H. Lee, H.-W. Lee, and B.-K. Kim, "Low temperature sintering of BaZrO₃-based proton conductors for intermediate temperature solid oxide fuel cells," *Solid State Ionics*, **181**, 163-7 (2010).
- ²⁹E. Fabbri, A. D'Epifanio, E. Di Bartolomeo, S. Licoccia, and E. Traversa, "Tailoring the chemical stability of Ba(Ce_{0.8-x}Zr_x)Y_{0.2}O_{3-d} protonic conductors for Intermediate Temperature Solid Oxide Fuel Cells (IT-SOFCs)," *Solid State Ionics*, **179**, 558-64 (2008).
- ³⁰ASTM E384, Standard test method for microhardness of materials, 1984.
- ³¹K. Niihara, R. Morena, and D. P. H. Hasselman, "Evaluation of K_{IC} of brittle solids by the indentation method with low crack-to-indent ratios," *J. Mater. Sci. Lett.*, **1**, 13-6 (1982).
- ³²G. D. Quinn, and R. C. Bradt, "On the Vickers Indentation Fracture Toughness Test," *J. Amer. Ceram. Soc.*, **90**, 673-80 (2007).
- ³³P. I. Dahl, H. L. Lein, Y. Yu, J. Tolchard, T. Grande, M.-A. Einarsrud, C. Kjølseth, T. Norby, and R. Haugsrud, "Microstructural characterization and electrical properties of spray pyrolyzed conventionally sintered or hot-pressed BaZrO₃ and BaZr_{0.9}Y_{0.1}O_{3-δ}," *Solid State Ionics*, **182**, 32-40 (2011).
- ³⁴E. Rocha-Rangel, *Fracture Toughness Determinations by Means of Indentation Fracture*. (InTech, 2010).
- ³⁵K. Harada, A. Shinya, D. Yokoyama, and A. Shinya, "Effect of loading conditions on the fracture toughness of zirconia," *Journal of Prosthodontic Research*, **57**, 82-7 (2013).
- ³⁶J. Kübler, "Fracture Toughness of Ceramics Using the SEVNB Method," (VAMAS, 1999).
- ³⁷I. J. McCole, *Ceramic hardness*. (Plenum Press, New York, 1990).
- ³⁸P. G. Sundell, M. E. Björketun, and G. Wahnström, "Thermodynamics of doping and vacancy formation in BaZrO₃ perovskite oxide from density functional calculations," *Physical Review B*, **73**, 104112 (2006).
- ³⁹Y. Yamazaki, C.-K. Yang, and S. M. Haile, "Unraveling the defect chemistry and proton uptake of yttrium-doped barium zirconate," *Scripta Materialia*, **65**, 102-7 (2011).
- ⁴⁰M. D. Goncalves, P. S. Maram, R. Muccillo, and A. Navrotsky, "Enthalpy of formation and thermodynamic insights into yttrium doped BaZrO₃," *J. Mater. Chem. A*, **2**, 17840-7 (2014).
- ⁴¹K. N. Marushkin, G. D. Nipan, and V. B. Lazarev, "Thermodynamics and (p,T,x) phase diagram of (barium oxide + diyttrium trioxide)," *J. Chem. Thermodynamics*, **27**, 465-74 (1995).
- ⁴²A. R. Cooper, *Mass Transport Phenomena in Ceramics*. (Plenum Press, New York, 1975).
- ⁴³S. Yamanaka, M. Fujikane, T. Hamaguchi, H. Muta, T. Oyama, T. Matsuda, S.-i. Kobayashi, and K. Kurosaki, "Thermophysical properties of BaZrO₃ and BaCeO₃," *J. All. and Comp.*, **359**, 109-13 (2003).
- ⁴⁴R. Vassen, X. Cao, F. Tietz, D. Basu, and D. Stöver, "Zirconates as New Materials for Thermal Barrier Coatings," *Journal of the American Ceramic Society*, **83**, 2023-8 (2000).
- ⁴⁵T. Maekawa, K. Kurosaki, and S. Yamanaka, "Thermal and mechanical properties of perovskite-type barium hafnate," *J. All. and Comp.*, **407**, 44-8 (2006).
- ⁴⁶G. Panomsuwan, O. Takai, and N. Saito, "Optical and mechanical properties of transparent SrTiO₃ thin films deposited by ECR ion beam sputter deposition," *Physica Status Solidi (a)*, **210**, 311-9 (2013).
- ⁴⁷W. Ma, D. E. Mack, R. Vaßen, and D. Stöver, "Perovskite-Type Strontium Zirconate as a New Material for Thermal Barrier Coatings," *Journal of the American Ceramic Society*, **91**, 2630-5 (2008).
- ⁴⁸F. Dogan, and P. N. Kumta, *Advances in Electronic and Electrochemical Ceramics: Proceedings of the 107th Annual Meeting of The American Ceramic Society*. (John Wiley & Sons, 2012).
- ⁴⁹D. Hassan, S. Janes, and R. Clasen, "Proton-conducting ceramics as electrode/electrolyte materials for SOFC's—part I: preparation, mechanical and thermal properties of sintered bodies," *J. Eur. Ceram. Soc.*, **23**, 221-8 (2003).
- ⁵⁰H. Yang, Y. Ohishi, K. Kurosaki, H. Muta, and S. Yamanaka, "Thermomechanical properties of calcium series perovskite-type oxides," *J. All. and Comp.*, **504**, 201-4 (2010).
- ⁵¹A. K. Eriksson Andersson, S. M. Selbach, C. S. Knee, and T. Grande, "Chemical Expansion Due to Hydration of Proton-Conducting Perovskite Oxide Ceramics," *Journal of the American Ceramic Society*, **97**, 2654-61 (2014).

⁵²A. K. Eriksson Andersson, S. M. Selbach, T. Grande, and C. S. Knee, "Thermal evolution of the crystal structure of proton conducting $\text{BaCe}_{0.8}\text{Y}_{0.2}\text{O}_{3-\delta}$ from high-resolution neutron diffraction in dry and humid atmosphere," *Dalton Transactions*, **44**, 10834-46 (2015).

⁵³B. Lawn, *Fracture of Brittle Solids*. Cambridge solid state science series (ed. 2nd, 1993).

Tables

Table 1. Sintering temperature, density, cell parameters, average grain size, Vickers hardness and fracture toughness of $\text{BaZr}_{1-x}\text{Y}_x\text{O}_{3-\delta}$ and $\text{BaCe}_{0.2}\text{Zr}_{0.7}\text{Y}_{0.1}\text{O}_{2.95}$ ceramics. Sintering time was 10 h. *Italic:* Vickers hardness and fracture toughness after exposure to synthetic air at 650 °C for 10 h.

Compound	T _{sintering} (°C)	Density (%)	Cell parameter (Å)	Average grain size (µm)	Vickers Hardness (H _v)	Fracture toughness (MPa·m ^{1/2})
BZ	1600	97±1	4.1931±0.0001	0.99±0.14	868±23 <i>867±33</i>	1.81±0.18 <i>1.78±0.09</i>
BZY5	1600	95±1	4.1953±0.0001	0.18±0.01	946±34 <i>951±18</i>	1.84±0.12 <i>1.83±0.04</i>
BZY10_1600	1600	95±2	4.1981±0.0001	0.24±0.01	895±19 <i>884±13</i>	1.86±0.05 <i>1.80±0.1</i>
BZY10_1700	1700	95±1	4.1978±0.0001	0.61±0.02	1049±22 <i>1042±28</i>	1.82±0.07 <i>1.85±0.04</i>
BZY10_1600*	1600	95±1	4.2074±0.0001	0.52±0.04	742±7	1.58±0.13
BZY20	1600	95±2	4.2151±0.0001	0.64±0.03	801±20 <i>805±11</i>	1.79±0.08 <i>1.81±0.08</i>
BCZY27_1600	1600	95±2	4.2494±0.0001	0.28±0.04	858±21 <i>857±13</i>	1.65±0.11 <i>1.64±0.06</i>
BCZY27_1700	1700	95±1	4.2492±0.0001	0.63±0.07	842±15 <i>844±22</i>	1.56±0.07 <i>1.55±0.07</i>
BCZY27_1600*	1600	94±1	4.2509±0.0001	0.7±0.08	734±23	1.46±0.03

Figure captions

Fig. 1. SEM micrographs of barium zirconate materials conventionally sintered at 1600 °C for 10 h in air: a.) BZ; b) BZY5; c) BZY10; d) BZY20; e) BCZY27.

Fig. 2. SEM image of a typical indent on pristine BCZY27 with the insets of indentation scheme, crack-start and crack-end.

Fig. 3. Effect of the indentation load on the Vickers hardness of pristine BZY10. Inset: effect of indentation load on the fracture toughness of pristine BZY10.

Fig. 4. SEM images of the indents on $\text{BaZr}_{0.9}\text{Y}_{0.1}\text{O}_{2.95}$ (BZY10) samples, (a) pristine and exposed to flowing CO_2 atmosphere for 10 h at (b) 550 °C, (c) 650 °C and (d) 750 °C. Insets: BaCO_3 crystals formed on the surface and crack-ends after indentation on the ceramics exposed to CO_2 .

Fig. 5. XRD patterns of $\text{BaZr}_{0.9}\text{Y}_{0.1}\text{O}_{2.95}$ (BZY10) before and after exposure to flowing CO_2 atmosphere at 650 °C for 10 and 20 h. The XRD source is not completely monochromatic and the diffraction line at $\sim 29^\circ$ is due to W radiation. Diffraction pattern of Au is due to sputtered Au on the surface prior to electron microscopy. Inset: left - (111) diffraction peak of BaCO_3 ; right – GIXD of BZY10 exposed to CO_2 at 650 °C for 10 h.

Fig. 6. SEM image of the cross section of BZY10 and EDS line scans of elements Zr, Ba, Y across from the surface exposed to CO_2 towards the bulk. The line scan was performed in parallel to the direction of the Vickers indent.

Fig. 7. SEM images of indents on (a) BZ, (b) BZY5, (c) BZY20, and (d) BCZY27 with BaCO_3 formed after exposure to pure CO_2 at 650 °C for 10 h. Insets: crack-ends after indentation on exposed ceramics.

Fig. 8. SEM images of indents on (a), (b), (c), (d) $\text{BaZr}_{0.9}\text{Y}_{0.1}\text{O}_{2.95}$ (BZY10) and (e), (f), (g), (h) $\text{BaCe}_{0.2}\text{Zr}_{0.7}\text{Y}_{0.1}\text{O}_{2.95}$ (BCZY27) samples before (left column) and after (right column) exposure to pure CO_2 at 650 °C for 10 h. Samples: (a), (b), (e), (f) sintered at 1600 °C and additionally annealed at 1700 °C; (c), (d), (g), (h) sintered with sacrificial powder at 1600 °C. Insets: crack-ends, crack-starts after indentation and BaCO_3 crystals on the surface.

Fig. 9. Effect of CO_2 exposure temperature on Vickers hardness and fracture toughness of (a), (b) $\text{BaZr}_{0.9}\text{Y}_{0.1}\text{O}_{2.95}$ (BZY10) and (c), (d) $\text{BaCe}_{0.2}\text{Zr}_{0.7}\text{Y}_{0.1}\text{O}_{2.95}$ (BCZY27) samples sintered at 1600 °C, annealed at 1700 °C and sintered at 1600 °C with sacrificial powder before and after exposure to pure CO_2 and synthetic air for 10 h.

Fig. 10. Effect of exposure temperature in pure CO_2 for 10 h on (a) Vickers hardness and (b) fracture toughness for $\text{BaZr}_{1-x}\text{Y}_x\text{O}_{3-x/2}$ and $\text{BaCe}_{0.2}\text{Zr}_{0.7}\text{Y}_{0.1}\text{O}_{2.95}$ specimens conventionally sintered at 1600 °C.

Fig. 11. An illustration of the microstructural changes on the surface of BZ-ceramics due to reaction with CO_2 .

Fig. 12. (a) Stable region plot of some BZ-materials at different CO_2 partial pressures and temperatures obtained by thermodynamic calculations; (b) The equilibrium reaction temperature of different $\text{BaZr}_{1-x}\text{Y}_x\text{O}_{3-x/2}$ with CO_2 as a function of composition and CO_2 partial pressures; CO_2 partial pressure in atm as indicated. The data for calculations is taken from literature.^{18, 19, 40, 41}